Decoupled and Closed-Loop Motion and Stiffness Control for Articulated Soft Robots Driven by a Class of Electromechanical Variable Stiffness Actuators

Maja Trumić, *Member, IEEE*, Franco Angelini, *Member, IEEE*, Kosta Jovanović, *Member, IEEE*, and Adriano Fagiolini, *Senior Member, IEEE*

***Abstract*—Controlling articulated soft robots (ASRs) driven by variable stiffness actuators (VSAs) remains an open challenge from the model-based control perspective, where the key difficulties are due to: 1) the coupling between motion and stiffness dynamics; 2) highly nonlinear dynamics; and 3) sensitivity to the model accuracy. Herein, we contribute to: 1) by achieving decoupling through shifting the eigenvalues of the actuator matrix to avoid singularity, followed by the compensation of such shift through the integral action. To address; 2) we design a cascade-based control that formally proves convergence of the motion and stiffness tracking errors to zero. Finally, our contribution resolves; and 3) by ensuring robustness to uncertain dynamics parameters through adaptive approach. Notably, this methodology enables independent motion and stiffness control design, allowing the application of diverse control strategies. The proposed solution is validated in simulation and on an ASR hardware setup. The results prove that the method is capable of controlling motion and stiffness in a decoupled manner, while the adaptive strategy ensures improved tracking performance.**

***Index Terms*—Adaptive control, motion control, soft robotics.**

I. Introduction

ARTICULATED soft robots (ASRs), i.e., robots with compliant actuation, that are driven by variable stiffness actuators (VSAs) (Fig. 1) have the capability to vary their joints' position and stiffness in real time, thus achieving performance comparable to biological systems [1]. In this domain, antagonistic VSAs are widely employed [2], [3], [4], [5] as they are characterized by a simpler mechanical design than other VSAs. However, their less complex mechanism comes at the expense of requiring a more sophisticated controller [6].

Received 8 February 2025; revised 25 July 2025; accepted 8 November 2025. Date of publication 19 December 2025; date of current version 25 February 2026. This work was supported in part by the European Union's Horizon Europe Marie Skłodowska-Curie Action "iMARS-Intelligent Multi Agent Robotic Systems" under Grant 101182996; in part by the European Union's Horizon Europe Marie Skłodowska-Curie Action Postdoctoral Fellowship "Soft-Scout-Controlling Soft Robots for Advanced Adaptivity and Versatility in Confined Spaces" under Grant 101202085; in part by Italian Ministry of Education and Research in the Framework of the Future-Oriented Research Laboratory (FoReLab) Project (Departments of Excellence); and in part by Serbian Ministry of Science, Technological Development and Innovation under Grant 451-03-136/2025-03/200103. The work was partly done in the Palace of Science, Miodrag Kostić Endowment. Recommended by Associate Editor C. Yang. *(Corresponding author: Adriano Fagiolini.)*

Maja Trumić is with Delft University of Technology, 2628 Delft, The Netherlands (e-mail: m.trumic@tudelft.nl).

Franco Angelini is with the Centro di Ricerca "Enrico Piaggio" and the Dipartimento di Ingegneria dell'Informazione, Università di Pisa, 56122 Pisa, Italy (e-mail: franco.angelini@unipi.it).

Kosta Jovanović is with the School of Electrical Engineering, University of Belgrade, 11000 Belgrade, Serbia (e-mail: kostaj@etf.rs).

Adriano Fagiolini is with MIRPALab, Department of Engineering, University of Palermo, 90128 Palermo, Italy (e-mail: fagiolini@unipa.it).

Digital Object Identifier 10.1109/TCST.2025.3637320

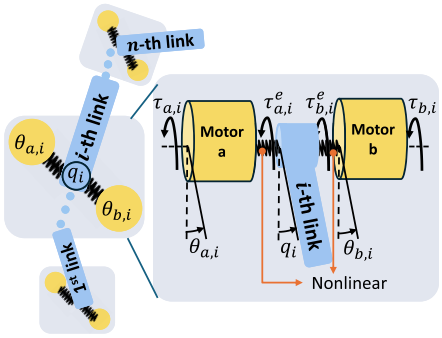

Fig. 1. Illustration of an ASR with n rigid links and n compliant joints driven by electromechanical antagonistic VSAs. A nonlinear torque-deflection relation enables real-time stiffness variation. The symbols represent motor positions $\theta_{a,i}$ and $\theta_{b,i}$, link position q_i, input motor torques $\tau_{a,i}$ and $\tau_{b,i}$, and elastic torques $\tau^e_{a,i}$ and $\tau^e_{b,i}$ for the ith joint.

Foremost, the control task is challenging due to the VSA's highly nonlinear elastic elements [7] and strong dynamic coupling between motion and stiffness [8], being undesired since varying stiffness can jeopardize precise motion tracking. Various control techniques have been proposed for ASRs with VSAs, ranging from model-free solutions, such as iterative learning control [9], [10], optimal [5], [11], and data-driven approach [12], to model-based ones such as feedback linearization [13], backstepping [14], elastic structure preserving control [15], [16], and observer-based control [17].

We propose a novel strategy for controlling ASRs that achieves simultaneous, independent and closed-loop tracking of link motion (position and velocity) and joint stiffness using a cascade-based control design. We consider here the internal, passive stiffness of a rotational robot joint, physically representing the amount of elastic torque change required to deform the elastic transmission from its current value. Our solution aligns with the philosophy of [8], where both motion and stiffness are controlled in the closed loop through a feedback linearization approach. However, compared to approaches, such as feedback linearization [13] and backstepping [14], which require precise knowledge of the model, we use adaptive control strategy [18] to relax the need for the precise parameters knowledge, being motivated by its superior performance when applied on soft robots [19], [20], [21]. Additionally, we leverage a dead-zone technique to make the system robust also to nonparametric uncertainties. Thus, the first contribution is the design of a control strategy that is robust to uncertainties.

Model-free solutions [9], [10], [12] can successfully deal with the system's high nonlinearity; however, it is challenging to prove the system's stability and they rely on repeated trials or prior identification. Furthermore, strategies, such as

observer-based control [17], neglect motor dynamics while proving stability. Thus, as a second contribution, we derive a formal stability proof for the overall VSA system, leveraging an adaptive approach to learn in real time and avoid prior identifications.

To address strong motion-stiffness coupling, a recent study approximates the elastic torque with a linear function and achieves simultaneous control of the joint's motion and the VSA's elastic elements pretension [16], while Mengacci et al. [10] reformulate the model to show that motion and adjusting dynamics can be decoupled under certain assumptions. However, neither solution explicitly controls the joint's stiffness. In contrast, our third contribution enables simultaneous and decoupled control of motion and stiffness dynamics.

Summary of Contributions:

1) We decouple motion and stiffness control by modifying the inverse actuation matrix and incorporating a compensating integral action, laying the groundwork for future research into alternative control techniques beyond the proposed adaptive strategy.
2) We design a cascade-based controller for a class of VSAs, proving as well stability of the overall closed-loop system.
3) We achieve robustness to uncertainties by leveraging the nonlinear adaptive control theory. By conducting simulation and experimental verification on the one-, two-, and three-degree-of-freedom (DoF) VSA-driven ASRs, we prove the efficacy of the proposed control strategy in accurately and independently tracking desired motion and stiffness references.

II. Dynamic Model and Problem Statement

An n-DoF robot with compliant joints, driven by electromechanical VSAs, is described by the agonist and antagonist motor position vectors $q_j = (q_{j,1}, \dots, q_{j,n})^\top$ for $j \in \{a, b\}$, and the link position vector $q = (q_1, \dots, q_n)^\top$ (Fig. 1). Each joint is actuated by input torques $\tau_{j,i}$ and characterized by transmission deflections $\phi_{j,i} = q_i - q_{j,i}$, generating local elastic torques $\tau^e_{j,i}$ for $i \in \{1, n\}$. The total elastic torque driving the ith link is given by their sum. The ASR system dynamics, with a detailed derivation provided in [22], are

$$\begin{aligned} B(q)\ddot{q} + C(q,\dot{q})\dot{q} + G(q) + \tau^e(\phi_a, \phi_b) &= \tau_{\text{ext}} \\ B_j\ddot{q}_j + D_j\dot{q}_j - \tau^e_j(\phi_j) &= \tau_j \end{aligned} \tag{1}$$

where $B(q), C(q,\dot{q}) \in \mathbb{R}^{n\times n}$ are the inertia and Coriolis matrices (including viscous friction and centrifugal terms), $G(q) \in \mathbb{R}^n$ is the gravity vector, $B_j = \text{diag}(b_{i,j})$ and $D_j = \text{diag}(d_{i,j})$ are the diagonal motor inertia and damping matrices, $\phi_j = (\phi_{j,1}, \dots, \phi_{j,n})^\top$, and $\tau_j = (\tau_{j,1}, \dots, \tau_{j,n})^\top$. The following properties hold.

Property 1: $B(q)$ is symmetric, uniformly positive definite, and bounded for any $q \in \mathbb{R}^n$, which implies $B^{-1}(q)$ always exists and is bounded [18].

Property 2: Matrix $\dot{B}(q) - 2C(q,\dot{q})$ is skew symmetric, which implies $v^\top(\dot{B}(q) - 2C(q,\dot{q}))v = 0$, for all v.

Property 3: The link regressor matrix, $Y(q,\dot{q},\ddot{q})$ (see [23], Sec. 7.3.2) and the block-diagonal motor regressor matrices, $Y_j = \text{diag}_i\{(\dot{q}_{j,i}\ \ddot{q}_{j,i})\} \in \mathbb{R}^{n\times 2n}$, for $j \in \{a, b\}$, allow expressing the following:

$$\begin{aligned} B(q)\ddot{q} + C(q,\dot{q})\dot{q} + G(q) &= Y(q,\dot{q},\ddot{q})\pi \\ B_j\ddot{q}_j + D_j\dot{q}_j &= Y_j(\dot{q}_j, \ddot{q}_j)\pi_j \end{aligned}$$

where $\pi_j = (d_{j,1}, b_{j,1}, \dots, d_{j,n}, b_{j,n})^\top$ and π is a suitable link parameter vector.

Property 4: The system (1) has elastically decoupled joints. Thus, its elastic potential energy can be expressed for each joint individually as $U^e_i = \sum_j U^e_{j,i}(\phi_{j,i})$ and the total elastic torque τ^e_i depends only on the local deflections, i.e., $\tau^e_i = \tau^e_{a,i}(\phi_{a,i}) + \tau^e_{b,i}(\phi_{b,i})$ [10]. Moreover, each term of the joint stiffness vector $\sigma = (\sigma_1, \dots, \sigma_n)^\top$ is defined as $\sigma_i = \partial\tau^e_{a,i}/\partial\phi_{a,i} + \partial\tau^e_{b,i}/\partial\phi_{b,i}$ [22], [24][1] and its time derivative is

$$\dot{\sigma}_i = \left(\partial^2\tau^e_{a,i}/\partial\phi^2_{a,i}\right)\dot{\phi}_{a,i} + \left(\partial^2\tau^e_{b,i}/\partial\phi^2_{b,i}\right)\dot{\phi}_{b,i}. \tag{2}$$

A further property helps in achieving decoupled control, by ensuring that both motion and stiffness dynamics share the same control inputs, i.e., local elastic torques.

Property 5: Elastic torques within a VSA are such that

$$\partial^2\tau^e_{j,i}/\partial\phi^2_{j,i} = \nu_{j,i}\tau^e_{j,i}, \quad \text{for } j \in \{a, b\} \tag{3}$$

where $\nu_{j,i}$ are the suitable scalars.

Meeting this requirement, i.e., ensuring that each $\tau^e_{j,i}$ solves (3), guarantees that τ^e_i is an exponential function of the local deflections. By the linearity of (2), this result translates also to the ith joint stiffness' dynamics. VSAs that satisfy the foregoing property are indeed quite common [4], as they are inspired by the behavior of biological muscles. Numerous examples include commercial VSAs with sine-hyperbolic elastic torque [25] and VSAs with the exponential springs [26], [27], [28], [29], [30].

Having said that, the full dynamics of the robot, including that of the joint stiffness, is

$$B(q)\ddot{q} + C(q,\dot{q})\dot{q} + G(q) + \tau^e_a(\phi_a) + \tau^e_b(\phi_b) = 0 \tag{4a}$$

$$\dot{\sigma}_i = \nu_{a,i}\tau^e_{a,i}(\phi_{a,i})\dot{\phi}_{a,i} + \nu_{b,i}\tau^e_{b,i}(\phi_{b,i})\dot{\phi}_{b,i} \quad \forall i \tag{4b}$$

$$B_j\ddot{q}_j + D_j\dot{q}_j - \tau^e_j(\phi_j) = \tau_j. \tag{4c}$$

The above system is underactuated as q_j, for $j \in \{a, b\}$ are collocated variables that are directly controlled via the inputs τ_j, while q and σ are noncollocated variables and only indirectly controlled via the elastic torques τ^e_j.

To this respect, the following final property is assumed.

Property 6: The mapping $\tau^e_{i,j} = f(q_i - q_{i,j})$ between elastic torques and motor positions is smooth and invertible, which implies that one can always write $q_{j,i} = q_i - f^{-1}(\tau^e_{j,i})$.

One can now readily introduce the following problem.

Problem 1: Given a VSA-driven robot with nominal model as in (4), design a *robust* control law for the input torque τ_a and

[1]More details on github.com/maja-trumic/adaptive-control-vsa

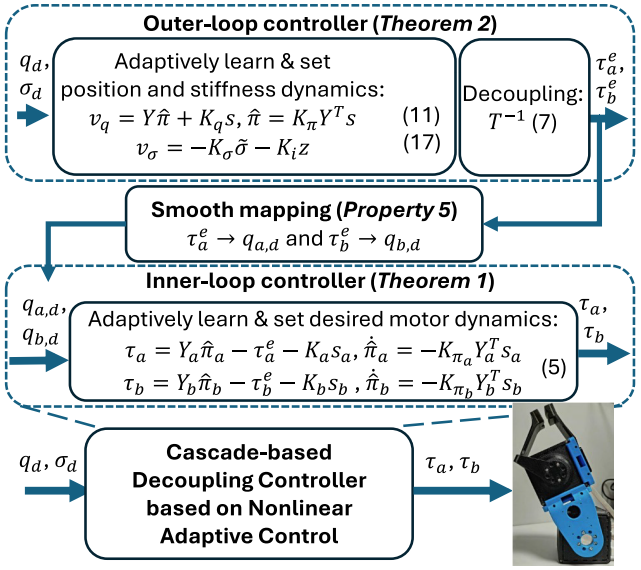

Fig. 2. Block scheme of the proposed nonlinear adaptive control-based control algorithm for the decoupled motion and stiffness control of ASR.

τ_b that allow desired motion and stiffness signals, q_d, $\dot{q}_d$, and σ_d, be asymptotically tracked, i.e., $\lim_{t\to\infty} \|q(t) - q_d(t)\| = 0$, $\lim_{t\to\infty} \|\dot{q}(t) - \dot{q}_d(t)\| = 0$, $\lim_{t\to\infty} \|\sigma(t) - \sigma_d\| = 0$, in a decoupled way. Robustness is intended with respect to parametric uncertainty in the vectors π and π_j, and decoupling refers to the ability to track q_d and $\dot{q}_d$ irrespective of σ_d and vice versa.

Below, $\mathbb{I}_n$ denotes the $n \times n$ identity matrix, $\mathbb{R}^n$ is the n-dimensional real vector space, $\mathbb{R}^{m\times n}$ is the space of $m \times n$ real matrices, and $\text{diag}_i\{A_i\}$ abbreviates $\text{diag}(A_1, \ldots, A_n)$, where A_i is the ith diagonal entry. A matrix $A \succ 0$ ($A \succeq 0$) is positive (semi)definite. A matrix $K = \text{diag}_i\{K_i\}$ is a *control gain* if $K \succ 0$.

III. Decoupled Nonlinear Adaptive Control of Electromechanically Driven ASR

Achieving decoupled control of link motion and joint stiffness is challenging due to system underactuation and strong coupling, while ensuring accuracy is further complicated by parametric uncertainties affecting both link and motor dynamics. This section presents the proposed strategy, which reaches robustness through a nonlinear adaptive control approach [18] and addresses underactuation via a cascade control scheme (Fig. 2). Specifically, an inner loop regulates motor positions to generate elastic torques (see Property 6), while an outer loop uses these torques to track user-specified position, velocity, and stiffness references. Property 3 is used below and parameter vectors are assumed constant or vary slowly.

Let us begin with describing the inner-loop control.

Theorem 1 (Inner-loop Nonlinear Adaptive Control): Given the actuator model in (4c) and desired signals $q_{j,d} : [0, \infty) \to \mathbb{R}^n$, with $q_{j,d} \in C^2$, for $j \in \{a, b\}$, global and robust asymptotic convergence of the tracking errors $\tilde{q}_j = q_j - q_{j,d}$ and $\tilde{\dot{q}}_j = \dot{q}_j - \dot{q}_{j,d}$ is guaranteed by the adaptive control law

$$\begin{aligned} \tau_j &= Y_j\left(q_j, \dot{q}_j, \ddot{q}_{j,d}\right)\hat{\pi}_j - \tau_j^e\left(\phi_j\right) - K_j s_j \\ \dot{\hat{\pi}}_j &= -K_{\pi_j} Y_j\left(q_j, \dot{q}_j, \ddot{q}_{j,d}\right)^\top s_j \end{aligned} \tag{5}$$

where $s_j = \dot{q}_j - \dot{q}_{j,r}$ and $\dot{q}_{j,r} = \dot{q}_{j,d} - \Lambda_j(q_j - q_{j,d})$, with $\Lambda \succ 0$, K_j and K_{π_j} are control gains, and where $Y_j = (\ddot{q}_{j,1,r}, \dot{q}_{j,1}, \ldots, \ddot{q}_{j,n,r}, \dot{q}_{j,n})$.

Proof: The proof shows the convergence of the motor tracking errors despite parametric uncertainty of the vectors π_j involved in Property 3. It assumes a dynamic control law is used that is based on motor parameter estimates $\hat{\pi}_j$, which are continuously updated. To this purpose, for each agonist and antagonist motor, consider the estimation errors of motor parameters $\tilde{\pi}_j = \hat{\pi}_j - \pi_j$, for $j \in \{a, b\}$ and the Lyapunov candidate $V_j = 1/2(s_j^\top B_j s_j + \tilde{\pi}_j^\top K_{\pi_j}^{-1}\tilde{\pi}_j)$. In the Lie derivative $\dot{V}_j = s_j^\top B_j \dot{s}_j + \dot{\tilde{\pi}}_j^\top K_{\pi_j}^{-1}\tilde{\pi}_j = s_j^\top B_j(\ddot{q}_j - \ddot{q}_{j,r}) + \dot{\hat{\pi}}_j^\top K_{\pi_j}^{-1}\tilde{\pi}_j$, replace $B_j\ddot{q}_j$ with its expression derived from (4c) and use Property 3, which leads to

$$\begin{aligned} \dot{V}_j &= s_j^\top\left(\tau_j + \tau_j^e\left(\phi_j\right) - D_j\dot{q}_j - B_j\ddot{q}_{j,r}\right) + \dot{\hat{\pi}}_j^\top K_{\pi_j}^{-1}\tilde{\pi}_j \\ &= s_j^\top\left(\tau_j + \tau_j^e\left(\phi_j\right) - Y_j\left(\dot{q}_j, \ddot{q}_{j,r}\right)\pi_j\right) + \dot{\hat{\pi}}_j^\top K_{\pi_j}^{-1}\tilde{\pi}_j \end{aligned}$$

with $\pi_j = (b_{j,1}, d_{j,1}, \ldots, b_{j,n}, d_{j,n})^\top$. Plugging the first laws in (5) gives $\dot{V}_j = s_j^\top(Y_j\tilde{\pi}_j - K_j s_j) + \dot{\hat{\pi}}_j^\top K_{\pi_j}^{-1}\tilde{\pi}_j \le -s_j^\top K_j s_j + (s_j^\top Y_j(\dot{q}_j, \ddot{q}_{j,r}) + \dot{\hat{\pi}}_j^\top K_{\pi_j}^{-1})\tilde{\pi}_j$, and selecting the parameter adaptation laws as in the second group of (5) results in the negative semidefinite function $\dot{V}_j = -s_j^\top K_j s_j$. To show that $s_j \to 0$ as $t \to \infty$, it suffices to prove that $\dot{V}_j \to 0$. Since $V_j \succ 0$, Barbalat's lemma ensures $\dot{V}_j \to 0$ if $\dot{V}_j$ is uniformly continuous. This holds if $\ddot{V}_j = -2\, s_j^\top K_j \dot{s}_j$ is bounded, requiring both s_j and $\dot{s}_j$ to be bounded. The boundedness of s_j follows from $V_j \succ 0$ and its nonincreasing nature ($\dot{V}_j \prec 0$), ensuring V_j remains bounded. To establish $\dot{s}_j$ bounded, note that $q_{j,d}$ are bounded. The closed-loop dynamics $\dddot{\tilde{q}}_j + K_{d,j}\ddot{\tilde{q}}_j + K_{p,j}\dot{\tilde{q}}_j = 0$ imply that $\ddot{\tilde{q}}_j$ is bounded, given that both $\tilde{q}$ and $\dot{\tilde{q}}_j$ are bounded. Thus, $\dot{s}_j$ is also bounded.□

With inner-loop convergence achieved, Property 6 ensures that the desired local elastic torques are reached, allowing us to proceed with the derivation of the outer-loop controller.

Theorem 2 (Outer-Loop Adaptive Control of Link Motion and Joint Stiffness): Given an ASR with dynamics as in (4a) and (4b) and desired vector signals $q_d, \sigma_d : [0, \infty) \to \mathbb{R}^n$, with $q_d \in \mathcal{C}^1$, global and robust asymptotic convergence of the tracking errors, $\tilde{q} = q - q_d$, $\tilde{\dot{q}} = \dot{q} - \dot{q}_d$ and $\tilde{\sigma} = \sigma - \sigma_d$, is guaranteed by the adaptive control law for the elastic torque

$$\begin{pmatrix} \tau_a^e \\ \tau_b^e \end{pmatrix} = T^{-1}(q, \dot{q}) \begin{pmatrix} Y(q, \dot{q}, \dot{q}_r, \ddot{q}_r)\hat{\pi} + K_q s \\ -K_\sigma\tilde{\sigma} - K_i z \end{pmatrix} \tag{6a}$$

$$\dot{\hat{\pi}} = K_\pi Y(q, \dot{q}, \dot{q}_r, \ddot{q}_r)^\top s \tag{6b}$$

where $s = \dot{q} - \dot{q}_r$, $\dot{q}_r = \dot{q}_d - \Lambda(q - q_d)$, with $\Lambda \succ 0$, $\dot{z} = \tilde{\sigma}$, Y is the link regressor, $\hat{\pi}$ is a link parameter estimate, and K_q, K_σ, K_i, and K_π are control gains, and

$$T = \begin{pmatrix} \mathbb{I}_n & \mathbb{I}_n \\ \text{diag}_i\left\{\nu_{a,i}\dot{\phi}_{a,i} + \Delta_i\right\} & \text{diag}_i\left\{\nu_{b,i}\dot{\phi}_{b,i} - \Delta_i\right\} \end{pmatrix} \tag{7}$$

where Δ_i is a small constant ensuring T is invertible.

Furthermore, given the parameter estimation error $\tilde{\pi} = \pi - \hat{\pi}$, a Lyapunov control function and its Lie derivative, ensuring uniform global asymptotic stability, are

$$\begin{aligned} V &= \frac{1}{2}\left(s^\top B(q)\, s + \tilde{\sigma}^\top\tilde{\sigma} + z^\top K_i z + \tilde{\pi}^\top K_\pi^{-1}\tilde{\pi}\right) \\ \dot{V} &= -s^\top K_q s - \tilde{\sigma}^\top K_\sigma\tilde{\sigma}. \end{aligned} \tag{8}$$

Proof:

1) *Compound Dynamics Derivation:* The link acceleration $\ddot{q}$ and stiffness dynamics can be factorized in terms of convenient inputs. Specifically, using (4) and having defined $v_q = (\mathbb{I}_n, \mathbb{I}_n)(\tau_a^{e\top}, \tau_b^{e\top})^\top$, one obtains

$$\begin{aligned}\ddot{q} &= -B(q)^{-1}\left(C(q,\dot{q})\dot{q} + G(q) + \tau_a^e + \tau_b^e\right)\\ &= -B(q)^{-1}\left(C(q,\dot{q})\dot{q} + G(q) + v_q\right).\end{aligned} \tag{9}$$

Defining then $v_\sigma = (\Gamma_a, \Gamma_b)(\tau_a^{e\top}, \tau_b^{e\top})^\top$, with $\Gamma_j = \mathrm{diag}_i\{v_{j,i}\dot{\phi}_{j,i}\}$, one obtains the stiffness dynamics

$$\dot{\sigma} = \begin{pmatrix} v_{a,1}\dot{\phi}_{a,1}\tau_{a,1}^e + v_{b,1}\dot{\phi}_{b,1}\tau_{b,1}^e \\ \vdots \\ v_{a,n}\dot{\phi}_{a,n}\tau_{a,n}^e + v_{b,n}\dot{\phi}_{b,n}\tau_{b,n}^e \end{pmatrix} = v_\sigma. \tag{10}$$

2) *Derivation of Control Inputs v_q and v_σ:* Expand the Lie derivative of the Lyapunov candidate $V = 1/2(s^\top B(q)s + \tilde{\sigma}^\top\tilde{\sigma} + \tilde{\pi}^\top K_\pi^{-1}\tilde{\pi})$

$$\begin{aligned}\dot{V} &= s^\top B(q)\,\dot{s} + \frac{1}{2}s^\top\dot{B}(q)\,s + \tilde{\sigma}^\top\dot{\tilde{\sigma}} + \tilde{\pi}^\top K_\pi^{-1}\dot{\tilde{\pi}}\\ &= -s^\top\left(B(q)\,\ddot{q}_r + C(q,\dot{q})\,\dot{q} + G(q) + v_q\right)\\ &\quad + \frac{1}{2}s^\top\dot{B}(q)\,s + \tilde{\sigma}^\top v_\sigma + \tilde{\pi}^\top K_\pi^{-1}\dot{\hat{\pi}}.\end{aligned}$$

Plugging the factorized link acceleration from (9) into $\dot{s} = \ddot{q} - \ddot{q}_r$, and that of the stiffness dynamics from (10), then using the skew-symmetry of $1/2\dot{B}(q) - C(q,\dot{q})\dot{q}$ (Property 2) leads to $\dot{V} = -s^\top(\alpha(q) + v_q) + \tilde{\sigma}^\top v_\sigma + \tilde{\pi}^\top K_\pi^{-1}\dot{\hat{\pi}}$, where $\alpha(q) = B(q)\ddot{q}_r + C(q,\dot{q})\dot{q}_r + G(q)$ and the assumption of a constant or slowly changing π has been done. Using Property 3 and the relation $\pi = \hat{\pi} - \tilde{\pi}$, one can rewrite $\alpha(q) = Y\hat{\pi} - Y\tilde{\pi}$, for suitable $Y = Y(q,\dot{q},\dot{q}_r,\ddot{q}_r)$. Then, the Lie derivative of V is written as $\dot{V} = -s^\top(Y\hat{\pi} + v_q) + \tilde{\sigma}^\top v_\sigma + \tilde{\pi}^\top(K_\pi^{-1}\dot{\hat{\pi}} + Y^\top s)$, where the equivalence $s^\top Y\tilde{\pi} = (s^\top Y\tilde{\pi})^\top = \tilde{\pi}^\top Y^\top s$ has been used. Now, one can now force $\dot{V}$ be equal the desired function $\dot{V}_d = -s^\top K_q s - \tilde{\sigma}K_\sigma\tilde{\sigma}$. Solving the equation $\dot{V} = \dot{V}_d$ for v_q, v_σ, and $\dot{\hat{\pi}}$ gives

$$v_q = Y(q,\dot{q},\dot{q}_r,\ddot{q}_r)\hat{\pi} + K_q s, \quad v_\sigma = -K_\sigma\tilde{\sigma} \tag{11}$$

and the parameter adaptation law (6b). As $s = \tilde{\dot{q}} + \Lambda\tilde{q} \to 0$, so it happens with $\tilde{q}$ and $\tilde{\dot{q}}$. Also, $\hat{\pi}$ remains bounded. Moreover, plugging the control input v_σ from (11) into the stiffness dynamics (10), we obtain $\dot{\sigma} = -K_\sigma\tilde{\sigma}$, by which each $\sigma_i \to \sigma_{d,i}$, for all i, with a convergence speed of $k_{\sigma,i}$.

3) *Mapping the Control Inputs v_q and v_σ to Elastic Torques:* The control laws v_q and v_σ are mapped to the corresponding elastic torque signals by solving the system

$$T'\begin{pmatrix}\tau_a^e\\ \tau_b^e\end{pmatrix} = \begin{pmatrix}v_q\\ v_\sigma\end{pmatrix}, \quad \text{with } T' = \begin{pmatrix}\mathbb{I}_n & \mathbb{I}_n\\ \Gamma_a & \Gamma_b\end{pmatrix} \tag{12}$$

whose solvability requires T' be invertible. As all blocks in T' are square and with the same sizes and the in-diagonal blocks, $\mathbb{I}_n$ and Γ_b, commute with each other, one gets via Sylvester's rule [31]

$$|T'| = |\mathbb{I}_n\Gamma_b - \mathbb{I}_n\Gamma_a| = \mathrm{diag}_i\left\{v_{b,i}\dot{\phi}_{b,i} - v_{a,i}\dot{\phi}_{a,i}\right\}$$
$$= \Pi_{i=1}^n\left(v_{b,i}\dot{\phi}_{b,i} - v_{a,i}\dot{\phi}_{a,i}\right)$$

showing T' is not invertible if $v_{a,i}\dot{\phi}_{a,i} = v_{b,i}\dot{\phi}_{b,i}$ for any i.

4) *Perturbation Ensuring Invertibility of T':* To overcome the invertibility issue, an equation system as in (12) is solved, replacing T' with a perturbed yet invertible T. In determining how to obtain T, note that, while the primary goal is still to control both link motion and joint stiffness, motion tracking is typically more critical than stiffness tracking in most applications. Therefore, only the rows of T' related to the stiffness subsystem are perturbed. The choice

$$T = T' + \begin{pmatrix}0_n & 0_n\\ \Delta & -\Delta\end{pmatrix} = \begin{pmatrix}\mathbb{I}_n & \mathbb{I}_n\\ \Gamma_a + \Delta & \Gamma_b - \Delta\end{pmatrix} \tag{13}$$

where $\Delta = \mathrm{diag}_i\{\Delta_i\}$ and all Δ_i are (small) constants, serves the purpose. Observing that the upper-left block in T, $\mathbb{I}_n$, is invertible and assuming that its Schur complement in T (see [32, p. 44]), $M = \Gamma_b - \Delta - (\Gamma_a + \Delta)\mathbb{I}_n^{-1}\mathbb{I}_n = \Gamma_b - \Gamma_a - 2\Delta$, is also invertible, one gets

$$T^{-1} = \begin{pmatrix}\mathbb{I}_n + M^{-1}(\Gamma_a + \Delta) & -M^{-1}\\ -M^{-1}(\Gamma_a + \Delta) & M^{-1}\end{pmatrix}.$$

The (unique) solution of the perturbed system is

$$\left(\tau_a^{e\top}, \tau_b^{e\top}\right)^\top = T^{-1}\left(v_q^\top, v_\sigma^\top\right)^\top. \tag{14}$$

Plugging (14) into (12) and subtracting the unperturbed solution yields the calculation error $\epsilon = (\epsilon_q^\top, \epsilon_\sigma^\top)^\top$ due to perturbation

$$\epsilon = T'T^{-1}\begin{pmatrix}v_q\\ v_\sigma\end{pmatrix} - \begin{pmatrix}v_q\\ v_\sigma\end{pmatrix} = \left(\begin{pmatrix}\mathbb{I}_n & 0_n\\ T_{21} & T_{22}\end{pmatrix} - \mathbb{I}_{2n}\right)\begin{pmatrix}v_q\\ v_\sigma\end{pmatrix}$$

with $T_{21} = \Gamma_a + (\Gamma_a - \Gamma_b)M^{-1}(\Gamma_a + \Delta)$ and $T_{22} = \Gamma_b M^{-1} - \Gamma_a M^{-1}$. To express ϵ in terms of Δ, we factorize T_{21}, by adding and subtracting $2\Delta M^{-1}(\Gamma_a + \Delta)$, leading to $T_{21} = \Gamma_a - 2\Delta M^{-1}(\Gamma_a + \Delta) - MM^{-1}(\Gamma_a + \Delta) = -\Delta(\mathbb{I}_n + 2M^{-1}(\Gamma_a + \Delta))$. Similarly, adjusting $T_{22} - \mathbb{I}_n$ by adding and subtracting $2\Delta M^{-1}$ gives $T_{22} - \mathbb{I}_n = (\Gamma_b - \Gamma_a - 2\Delta)M^{-1} + 2\Delta M^{-1} - \mathbb{I}_n = MM^{-1} + 2\Delta M^{-1} - \mathbb{I}_n = 2\Delta M^{-1}$. Thus, the perturbation-induced calculation error is

$$\epsilon = \Delta\begin{pmatrix}0_n & 0_n\\ -\left(\mathbb{I}_n + 2M^{-1}(\Gamma_a + \Delta)\right) & 2M^{-1}\end{pmatrix}\begin{pmatrix}v_q\\ v_\sigma\end{pmatrix}$$

which expands to

$$\begin{aligned}\epsilon_q &= 0\\ \epsilon_\sigma &= \Delta\left(2M^{-1}v_\sigma - \left(\mathbb{I}_n + 2M^{-1}(\Gamma_a + \Delta)\right)v_q\right).\end{aligned}$$

Since v_q stabilizes motion tracking, it is accurately computed, ensuring $e \to 0$. However, v_σ retains a steady-state calculation error, $\epsilon_\sigma \to Av_\sigma$ and $A = 2\Delta M^{-1}$. As Δ and M are diagonal, $A = \mathrm{diag}_i\{2\Delta_i/(v_{b,i}\dot{\phi}_{b,i} - v_{a,i}\dot{\phi}_{a,i} - 2\Delta_i)\}$. When close to the singularity of T', i.e., $v_{a,i}\dot{\phi}_{a,i} \approx v_{b,i}\dot{\phi}_{b,i}$, the ith diagonal entry of A tends to -1, making $A \to -\mathbb{I}_n$. Away from singularity, A remains bounded but nonzero, leading to a small yet persistent steady-state stiffness error.

5) *Compensation by Integral Action and Final Version of the Controller:* Following the idea in [33], an

integral term is added to a new Lyapunov candidate W so as to reestablish the stiffness convergence. Let z be a newly introduced variable with dynamics $\dot{z} = \tilde{\sigma}$ and consider the Lyapunov candidate

$$W = \frac{1}{2}\tilde{\sigma}^\top\tilde{\sigma} + \frac{1}{2}z^\top K_i z \tag{15}$$

where K_i is a control gain. The Lie derivative of W

$$\dot{W} = \left(\tilde{\sigma}^\top, z^\top\right)\left(v_\sigma^\top, (K_i\tilde{\sigma})^\top\right)^\top \tag{16}$$

is made negative semidefinite and equal to

$$\dot{W} = \left(\tilde{\sigma}^\top, z^\top\right)\begin{pmatrix} -K_\sigma\tilde{\sigma} - K_i z \\ K_i\tilde{\sigma}\end{pmatrix} = -\tilde{\sigma}^\top K_\sigma\tilde{\sigma}$$

by choosing the control law $v_\sigma = -K_\sigma\tilde{\sigma} - K_i z$ with K_σ a control gain. The stiffness tracking error convergence is ensured despite $\dot{W}$ being only negative semi-definite as per LaSalle's invariance principle [34]. Namely, imposing the condition $\tilde{\sigma} = 0$ be invariant for the controlled system also implies $\dot{\sigma} = 0$; plugging the two conditions into $\dot{\sigma} = -K_\sigma\tilde{\sigma} - K_i z$, finally leads to $z = 0$. Finally, direct computation of the overall Lyapunov control function and its Lie derivative yields (8).□

A noteworthy observation is the following.

Corollary 1 (Decentralized Stiffness Control): The fact that each joint stiffness results only from local drives' motion and the diagonal form of $K_i = \text{diag}_i\{k_{i,i}\}$ and $K_\sigma = \text{diag}_i\{k_{\sigma,i}\}$ enables elementwise stiffness control via the laws $v_{\sigma,i} = -k_{\sigma,i}\tilde{\sigma}_i - k_{i,i}z_i$, $\dot{z}_i = \tilde{\sigma}_i$.

Remark 1: The proposed methodology accommodates diverse control techniques, as evident from (14). The decoupling matrix T enables independent design of motion and stiffness controllers via v_q and v_σ, facilitating future exploration of alternative approaches, such as model predictive control, optimal control [35], recurrent neural networks [36], adaptive neural networks [37], or a baseline computed torque control (CTC) [38], where $v_q = -C(q,\dot{q})\dot{q} - G(q) + B(q)(\Lambda\tilde{\dot{q}} + K_q s - \ddot{q}_d)$.

A. Stability Analysis

Analyzing the stability of the adaptive cascade control scheme requires writing model (4) in cascade form. To this aim, define $x_1 = (q^\top, \dot{q}^\top, \sigma^\top)^\top$, $x_2 = (q_a^\top, \dot{q}_a^\top, q_b^\top, \dot{q}_b^\top)^\top$, $\theta_1 = \pi$, and $\theta_2 = (\pi_a^\top, \pi_b^\top)^\top$, which yields $\dot{x}_1 = f_1(t, x_1, \theta_1) + g(t, x, \theta_1, \theta_2)$, $\dot{x}_2 = f_2(t, x_2, \theta_2)$, where $t \in \mathbb{R}_{\geq 0}$ and f_1, f_2, and g are Lipschitz in the state and piecewise continuous in time for θ_1 and θ_2. According to [39], the above model is uniformly semi-globally practically asymptotically stable (USPAS) for all parameter sets $\Theta_1 \subset \mathbb{R}^{m1}$ and $\Theta_2 \subset \mathbb{R}^{m2}$, if: 1) the dynamics of x_2 is USPAS on Θ_2; 2) $\dot{x}_1 = f_1(t, x_1, \theta_1)$ is USPAS and the solutions of x_1 converge irrespectively of the origin's attractive neighborhood; 3) the interconnection term g is as $|g(t, x, \theta_1, \theta_2)| \leq G(|x|)$, where $G : \mathbb{R}_{\leq 0} \to \mathbb{R}_{\leq 0}$ is a nondecreasing function; and 4) the model's solutions are uniformly bounded.

As for 1), Theorem 1 proves the uniform exponential stability of the closed-loop motor dynamics, which is a stricter condition than being USPAS. As for 2) and 4) can be validated by following the procedure in [39] and via the Lyapunov function in Theorem 2. As for 3), Property 1 allows proving that the entries of T are bounded, namely all Γ_j are bounded by the lemma in [39], which stands due to the triangle inequality $|\Gamma_j| = \nu_j|\dot{q} - \dot{q}_j| \leq \nu_j|\dot{q}| + \nu_j|\dot{q}_j|$.

TABLE I
NOMINAL PARAMETERS OF THE VSA-DRIVEN ROBOT

Link masses	$m_1 = m_2 = 0.45$ kg
Link inertias	$I_1 = I_2 = 0.0036$ kgm^2
Link lengths	$l_1 = l_2 = 0.09$ m
Agonistic motor param.	$k_a = 0.0227$ Nm, $a_a = 6.7328$ rad^{-1}
Antagonistic motor param.	$k_b = 0.0216$ Nm, $a_b = 6.9602$ rad^{-1}
Motor inertia & damping	$b = 10^{-3}$ kgm^2, $d = 10^{-6}$ Ns

IV. Method Application and Evaluation

This section consists of three parts: 1) derivation of the adaptive controller; 2) simulation results; and 3) experimental validation. The method is assessed through step response analysis, comparison with CTC, and robustness evaluation against disturbances.

A. Derivation of the Controller

1) Link Dynamics: Defining the robot's configuration vector as $q = (q_1, q_2)^\top$ and joint stiffness vector as $\sigma = (\sigma_1, \sigma_2)^\top$, the robot dynamics follow (4a) and (4b). The link dynamics is in [19] (see page 8) with parameters in Table I. Moreover, from (13), the actuation matrix is $T = \{T_{ik}\}_{ik}$, with $T_{11} = T_{12} = \mathbb{I}_2$, $T_{21} = \text{diag}_i\{a_a^2\dot{\phi}_{a,i} + \Delta_i\}$, and $T_{22} = \text{diag}_i\{a_b^2\dot{\phi}_{b,i} - \Delta_i\}$, where $\dot{\phi}_{j,i} = \dot{q}_i - \dot{q}_{j,i}$.

2) Actuation: For motor dynamics (4c), the inertia and damping matrices are $B_a = \text{diag}_i\{b_{a,i}\}$, $B_b = \text{diag}_i\{b_{b,i}\}$, $D_a = \text{diag}_i\{d_{a,i}\}$, and $D_b = \text{diag}_i\{d_{b,i}\}$, with parameters from Table I. According to [25], the ith VSA device applies an elastic torque and sets a joint stiffness as

$$\begin{aligned}\tau_i^e &= k_a \sinh\left(a_a\phi_{a,i}\right) + k_b \sinh\left(a_b\phi_{b,i}\right)\\ \sigma_i &= a_a k_a \cosh\left(a_a\phi_{a,i}\right) + a_b k_b \cosh\left(a_b\phi_{b,i}\right)\end{aligned} \tag{17}$$

where k_a, k_b, a_a, and a_b are experimentally identified spring constants (Table I). Expanding sinh as $\tau_i^e = k_a/2(^{a_a\phi_{a,i}} - ^{-a_a\phi_{a,i}}) + k_b/2(^{a_b\phi_{b,i}} - ^{-a_b\phi_{b,i}})$ shows Property 5 is met. Using (17), motor positions are $q_a = q - \text{asinh}\left(\tau_a^e/k_a\right)/a_a$ and $q_b = q - \text{asinh}\left(\tau_b^e/k_b\right)/a_b$, ensuring Property 6.

3) Regressors and Parameters: The link-side regressor and the parameter vector are in [19] (see page 8). The motor-side regressors are $Y_j = \text{diag}_i\{(\dot{q}_{j,i}, \ddot{q}_{j,i,r})\}$, for $i \in \{1, 2\}$ with parameter vectors $\pi_j = (d_{1,j}, b_{1,j}, d_{2,j}, b_{2,j})^\top$.

With the regressor matrices and parameter vectors defined and Properties 5 and 6 satisfied, the adaptive controller is obtained by substituting the elastic torque expressions from (6a) into the motor torque control law (5) and applying the corresponding parameter adaptation rules (5) and (6a).

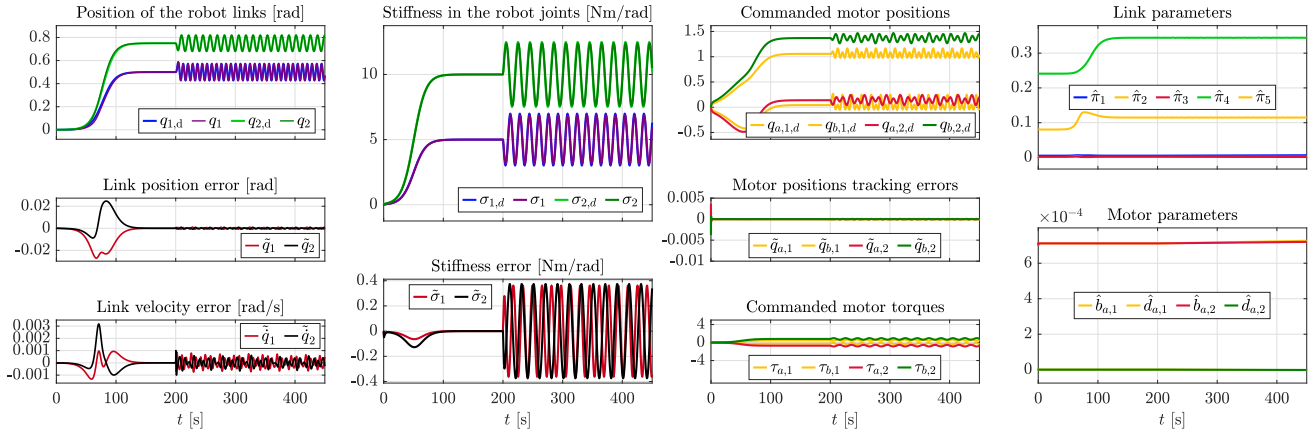

Fig. 3. Simulation run of a two-DoF electromechanical ASR with 30% parameters error. Position and stiffness references first converge to the constant values (for $t \in [0, 200)$) and then have a sinusoidal shape. After the initial transient, all references are asymptotically tracked with feasible torque commands, while the parameter estimations remain bounded. To avoid overcrowding the plot, we present only the evolution of one motor's parameters, as the other motor's parameters have identical estimation result, i.e., $\hat{b}_{b,1} = \hat{b}_{a,1}$, $\hat{d}_{b,1} = \hat{d}_{a,1}$, $\hat{b}_{b,2} = \hat{b}_{a,2}$, and $\hat{d}_{b,2} = \hat{d}_{a,2}$.

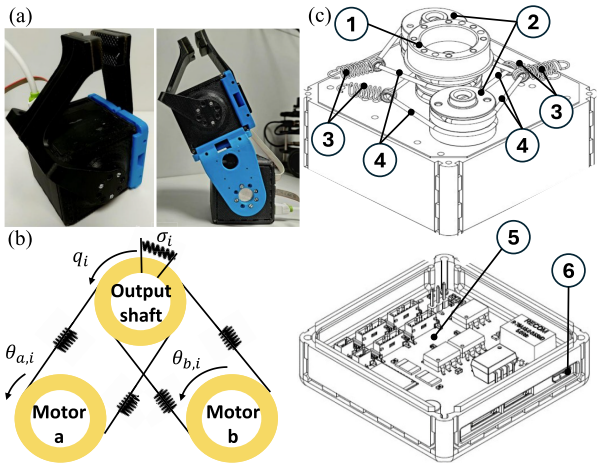

Fig. 4. Experimental setup. (a) One- and two-DoF hardware setups for validation. (b) Bidirectional antagonistic setup, where $\theta_{a,i}$ and $\theta_{b,i}$ are motor positions, σ_i is stiffness, and q_i is the ith joint's output position. Joint motion is achieved by rotating both motors in the same direction, while stiffness is adjusted by moving them oppositely. (c) Exploded VSA view showing: 1) output shaft; 2) pulleys; 3) four nonlinear springs; 4) four tendons; 5) a PCB with a Cypress PSoC 3 microcontroller handling motor control and position sensing via AS5045 encoders (12-bit); and 6) a micro-USB port for communication and firmware deployment.

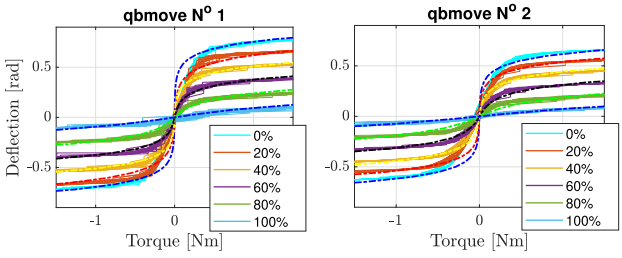

Fig. 5. Torque-deflection relations from repeated tests on two qbmove VSAs, later used in experiments, for stiffness presets from 0% to 100%. Experimental results overlap with the modeled torque-deflection relation (dashed lines). There is qualitatively consistent behavior with some hysteresis.

4) Robustness to Nonparametric Uncertainties: The adaptive control, designed for parametric uncertainties, may be affected by nonparametric uncertainties, such as measurement noise, hysteresis, or disturbances, which can cause parameter estimates to drift and potentially lead to instability. To mitigate this, we incorporate a dead-zone technique that prevents unnecessary parameter updates when tracking errors are small, as they are likely due to noise or disturbances. The parameter update law is kept as $\dot{\hat{\pi}} = K_\pi Y^\top s$ when $|s| > \eta$ and modified to $\dot{\hat{\pi}} = 0$ $|s| \leq \eta$, where η is the dead-zone threshold, chosen to balance accuracy and robustness.

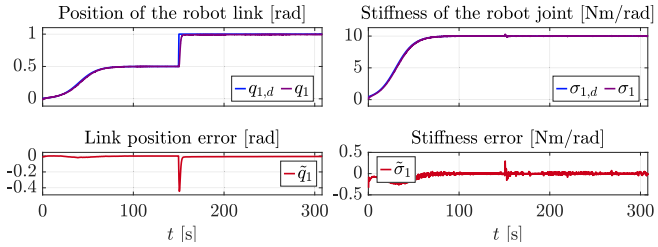

Fig. 6. Experimental run of a 1-DoF ASR when a position step is commanded. The position is accurately tracked, with stiffness exhibiting a short transient.

B. Simulation Validation

The approach is first tested in MATLAB/Simulink by introducing parametric uncertainties of 30% in the link and motor dynamics, relative to the nominal values reported in Table I. As shown in Fig. 3, desired signals, q_d and σ_d, are designed to include two phases: one where both signals are set to reach a constant value for $t \in [0, 200)$ (to evaluate steady-state performance) and another where they follow a sinusoidal trajectory $t \in [200, 450)$ (to assess trajectory tracking performance). During the sinusoidal phase, it holds: $q_{i,d} = \epsilon_{q_i} + A_{q_i} \sin \omega_{q_i} t$ and $\sigma_{i,d} = \epsilon_{\sigma_i} + A_{\sigma_i} \sin \omega_{\sigma_i} t$, where $\epsilon_{q_1} = 0.5$, $\epsilon_{q_2} = 0.75$, $A_{q_1} = 0.15$, $A_{q_2} = 0.1$, $\omega_{q_1} = \pi/4$, $\omega_{q_2} = \pi/6$, $\epsilon_{\sigma_1} = 5$, $\epsilon_{\sigma_2} = 10$, $A_{\sigma_1} = 2$, $A_{\sigma_2} = 2.5$, $\omega_{\sigma_1} = \pi/8$, and $\omega_{\sigma_2} = \pi/10$. Control gains are set to ensure a faster inner loop than the outer loop. Precisely, $K_{p,j} = \mathbb{I}_2$, $K_{d,j} = 0.1\mathbb{I}_2$, $K_q\Lambda = 0.8\mathbb{I}_2$, $K_q + \Lambda = 0.05\mathbb{I}_2$, $K_\sigma = 15\mathbb{I}_2$, $K_i = 20\mathbb{I}_2$, $\Delta = 70\mathbb{I}_2$, and $K_\pi = 20\mathbb{I}_2$. Fig. 3 confirms that both position and stiffness references are accurately tracked. Crucially, position

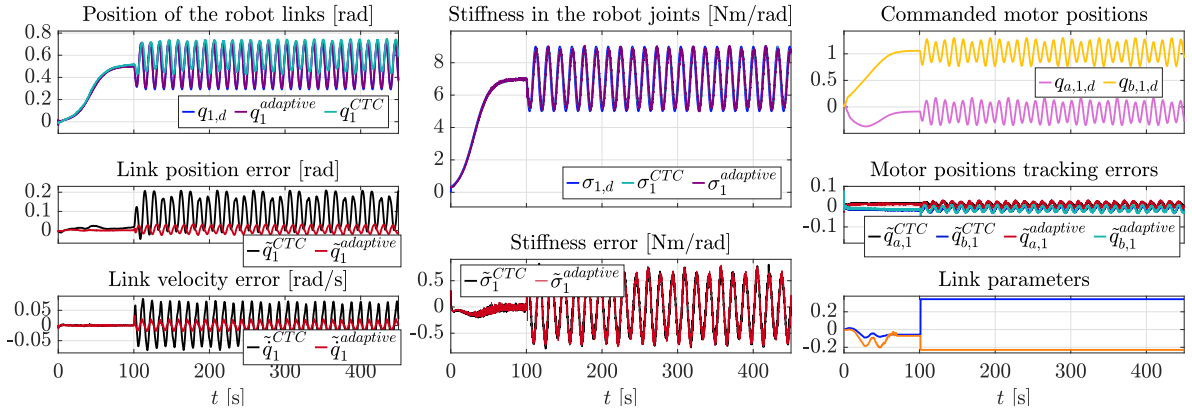

Fig. 7. Experimental run of a 1-DoF ASR using CTC and the proposed adaptive approach for motion tracking. The CTC leads to significant position and velocity tracking error due to the lack of robustness to uncertainties. With identical stiffness control in both cases, stiffness reliably reaches the desired setpoint and tracks the trajectory with bounded error. Commanded motor positions evolve smoothly in both cases.

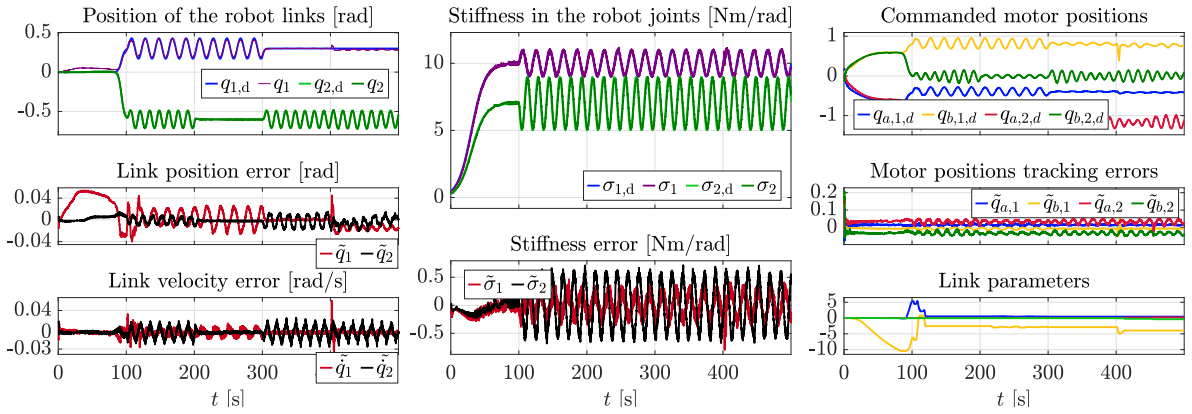

Fig. 8. Experimental run of a two-DoF ASR using the proposed control. Joint positions, velocities, and stiffnesses are accurately tracked, with bounded parameters and smooth commands. The leftmost figure shows decoupling, as link positions remain stable despite stiffness and other link variations. At 400 s, adding a load to the second link caused a brief tracking error, which was quickly compensated within the dead-zone bounds.

tracking remains unaffected by stiffness, and stiffness regulation is independent of position commands, demonstrating the desired decoupling. After the initial transient, the controller compensates for uncertainties. The figure also shows motor positions, tracking errors, torques, and parameters adaptation, that converge to constant values.

C. Experimental Validation

The proposed control approaches are finally validated using an ASR with VSAs in an antagonistic setup as in Fig. 4(a).

1) Hardware and Software Setup: The robot is an articulated arm with two revolute joints, each driven by an antagonistic VSA *qbmove Maker Pro* [25], whose hardware and software are open-source. This bidirectional antagonistic actuator allows each motor to apply both positive and negative torques [Fig. 4(b)]. The main mechanical and electronic components are shown in Fig. 4(c). Communication with the actuators is handled via MATLAB/Simulink libraries. Since the actuators feature embedded motor position control, input signals $q_{a,d}$ and $q_{b,d}$ are sent as motor position commands. The nominal geometric and inertial parameters of the robot are listed in Table I. The characterization of the actuators' torque-deflection relation follows the procedure in [40]. Fig. 5 illustrates the measured torque on the abscissa (using an ATI force/torque sensor) and the corresponding transmission deflection on the ordinate axis, computed as $q_i - (q_{a,i} + q_{b,i})/2$. These experimental data are used to fit the analytical elastic torque model in (17) (dashed line in Fig. 5), with parameters $k_1 = 0.006$, $a_1 = 7.14$, $k_2 = 0.001$, and $a_2 = 10.95$.

For validation, we first test a 1-DoF qbmove setup, followed by results on the 2-DoF system; experimental validation for the 3-DoF setup and the video are left on GitHub[1].

2) Experimental Results for the 1-DoF ASR: The closed-loop step response is first analyzed with a constant desired stiffness σ_d and a stepwise link position q_d (Fig. 6). The 1-DoF robot's dynamic model is $(I_1 + m_1 l_1^2)\ddot{q}_1 + m_1 g l_1 \sin q_1 + \tau_a^e + \tau_b^e = 0$, with the regressor matrix, $Y = (\ddot{q}_{1,r}, \sin q_1)$, and the unknown parameters $\pi = (I_1 + m_1 l_1^2, m_1 g l_1)^\top$. To facilitate parameter learning, the system initially follows a smooth, slow sigmoid trajectory, $q_d = 1/(2(1 + e^{-0.1t}))$. Once parameters are identified, a step command is applied at $t = 150$ s. The step response exhibits no oscillations or overshoot, with a rise time of $t_{\text{rise}} = 2.2$ s and a settling time of $t_{\text{settle}} = 3.8$ s (measured within 5% of the final value). The joint stiffness transient has a peak of 0.25 Nm/rad and settles in $t = 0.9$ s (within 2% of the reference).

Next, the proposed adaptive control is compared to the baseline CTC. The 1-DoF robot is commanded to first reach a

setpoint and then track a sinusoidal trajectory. The reference signals are described by $\epsilon_{q_1} = 0.5$, $A_{q_1} = 0.3$, $\omega_{q_1} = \pi/6$, $\epsilon_{\sigma_1} = 7$, $A_{\sigma_1} = 2$, and $\omega_{\sigma_1} = \pi/8$. These values ensure operation within manufacturer specifications [25]. The control gains for the CTC are $K_q\Lambda = 160^2$, $K_q + \Lambda = 320$, $K_\sigma = 10$, $K_i = 20$, and $\Delta = 105$, and for the adaptive control are $K_q\Lambda = 2.8$, $K_q + \Lambda = 0.4$, $K_\sigma = 10$, $K_i = 20$, $K_\pi = 10$, and $\Delta = 105$. Fig. 7 shows that adaptive control reduces position tracking error nearly tenfold by adapting parameters. Quantitatively, it achieves a root mean square error of 0.016 rad for position and 0.01 rad/s for velocity tracking, significantly outperforming the CTC (0.1 rad and 0.045 rad/s). The figure also shows smooth commanded and achieved motor positions, and parameter convergence.

3) Experimental Results for the 2-DoF ASR: We extend the analysis to a 2-DoF ASR using two *qbmove Maker Pro* actuators [Fig. 4(a)] to demonstrate decoupling and tracking. Joint positions remain constant in certain segments, while stiffness and the other joint's position vary. The references are described by $\epsilon_{q_1} = 0.3$, $\epsilon_{q_2} = -0.6$, $A_{q_1} = 0.15$, $A_{q_2} = 0.15$, $\omega_{q_1} = \pi/10$, $\omega_{q_2} = \pi/7$, $\epsilon_{\sigma_1} = 7$, $\epsilon_{\sigma_2} = 10$, $A_{\sigma_1} = 1$, $A_{\sigma_2} = 2$, $\omega_{\sigma_1} = \pi/8$, and $\omega_{\sigma_2} = \pi/10$. The first joint's stiffness is set higher to support the structure. Control gains are set as $K_q\Lambda = \text{diag}_i\{4.9\}$, $K_q + \Lambda = \text{diag}_i\{0.7\}$, $K_\sigma = \text{diag}_i\{10\}$, $K_i = \text{diag}_i\{20\}$, $K_\pi = \text{diag}_i\{10\}$, and $\Delta = \text{diag}_i\{105\}$. Fig. 8 confirms precise tracking and successful decoupling, as the position and velocity remain unaffected by stiffness changes or the other joint's movement. Also, we apply a disturbance at 400 s by placing an irregular object that weighs 0.25 kg on the end-effector. Parameters converge to the constant, but adapt when disturbed, keeping the error within $|s| \leq \eta = 0.1$.

D. Potential Applications

Our solution applies to the button-pushing task from [41], requiring accurate motion tracking to reach a button and precise stiffness regulation: too little stiffness prevents the button from being pushed, while too much may cause damage to the robot or the environment. It also holds promise for surgical robotic tasks, such as needle insertion. Moreover, its independent motion and stiffness control enables intuitive replication of human arm movement.

V. Conclusion

This article presents a nonlinear adaptive control strategy for robust and decoupled tracking of motion and stiffness in electromechanical ASRs. Decoupling is achieved by modifying the actuator matrix to ensure invertibility, while robustness is maintained through parameter adaptation and dead-zone technique. The approach is validated via simulations and experiments on a multi-DoF ASR, demonstrating accurate tracking. Stability is formally proven.

Future work will focus on extending to different VSAs, exploring alternative control laws and control variables, and addressing uncertainties in actuator mapping. Also, not closing the loop on acceleration and higher stiffness derivatives limits effectiveness in highly dynamic tasks, while their inclusion would improve control effectiveness.

References

[1] C. D. Santina et al., "Soft robots," in *Encyclopedia of Robotics*, vol. 489. Berlin, Germany: Springer, 2020.

[2] G. Milazzo, S. Lemerle, G. Grioli, A. Bicchi, and M. G. Catalano, "Design, characterization, and validation of a variable stiffness prosthetic elbow," *IEEE Trans. Robot.*, vol. 41, pp. 82–95, 2025.

[3] X. Sun, X. Xiong, W. Chen, W. Chen, and G. Yang, "Design and control of a novel variable stiffness actuator based on antagonistic variable radius principle," *ISA Trans.*, vol. 147, pp. 567–576, Apr. 2024.

[4] R. Mengacci, M. Garabini, G. Grioli, M. G. Catalano, and A. Bicchi, "Overcoming the torque/stiffness range tradeoff in antagonistic variable stiffness actuators," *IEEE/ASME Trans. Mechatronics*, vol. 26, no. 6, pp. 3186–3197, Dec. 2021.

[5] Y. Sun, Y. Tang, J. Zheng, D. Dong, and L. Bai, "Optimal variable stiffness control and its applications in bionic robotic joints: A review," *J. Bionic Eng.*, vol. 20, no. 2, pp. 417–435, Mar. 2023.

[6] B. Vanderborght et al., "Variable impedance actuators: A review," *Robot. Autonom. Syst.*, vol. 61, no. 12, pp. 1601–1614, 2013.

[7] S. Wolf et al., "Variable stiffness actuators: Review on design and components," *IEEE/ASME Trans. Mechatronics*, vol. 21, no. 5, pp. 2418–2430, Oct. 2016.

[8] A. De Luca, F. Flacco, A. Bicchi, and R. Schiavi, "Nonlinear decoupled motion-stiffness control and collision detection/reaction for the VSA-II variable stiffness device," in *Proc. IEEE/RSJ Int. Conf. Intell. Robots Syst.*, Oct. 2009, pp. 5487–5494.

[9] F. Angelini et al., "Decentralized trajectory tracking control for soft robots interacting with the environment," *IEEE Trans. Robot.*, vol. 34, no. 4, pp. 924–935, Aug. 2018.

[10] R. Mengacci, F. Angelini, M. G. Catalano, G. Grioli, A. Bicchi, and M. Garabini, "On the motion/stiffness decoupling property of articulated soft robots with application to model-free torque iterative learning control," *Int. J. Robot. Res.*, vol. 40, no. 1, pp. 348–374, Jan. 2021.

[11] S. P. Chhatoi, M. Pierallini, F. Angelini, C. Mastalli, and M. Garabini, "Optimal control for articulated soft robots," *IEEE Trans. Robot.*, vol. 39, no. 5, pp. 3671–3685, Oct. 2023.

[12] B. Lukić et al., "Cascade control of antagonistic VSA—An engineering control approach to a bioinspired robot actuator," *Frontiers Neurorobot.*, vol. 13, p. 69, Sep. 2019.

[13] G. Palli, C. Melchiorri, and A. De Luca, "On the feedback linearization of robots with variable joint stiffness," in *Proc. IEEE Int. Conf. Robot. Autom.*, May 2008, pp. 1753–1759.

[14] Y. Pan, Z. Zou, K. Guo, and C. Wen, "Analysis and verification on backstepping control of antagonistic variable stiffness actuators," *IEEE Robot. Autom. Lett.*, vol. 9, no. 12, pp. 11274–11281, Dec. 2024.

[15] M. Keppler, D. Lakatos, C. Ott, and A. Albu-Schäffer, "Elastic structure preserving (ESP) control for compliantly actuated robots," *IEEE Trans. Robot.*, vol. 34, no. 2, pp. 317–335, Apr. 2018.

[16] M. Harder, M. Keppler, X. Meng, C. Ott, H. Höppner, and A. Dietrich, "Simultaneous motion tracking and joint stiffness control of bidirectional antagonistic variable-stiffness actuators," *IEEE Robot. Autom. Lett.*, vol. 7, no. 3, pp. 6614–6621, Jul. 2022.

[17] S. Pedone, M. Trumic, K. Jovanovic, and A. Fagiolini, "Robust and decoupled position and stiffness control for electrically-driven articulated soft robots," *IEEE Robot. Autom. Lett.*, vol. 7, no. 4, pp. 9059–9066, Oct. 2022.

[18] J.-J. E. Slotine et al., *Applied Nonlinear Control*, vol. 199. Upper Saddle River, NJ, USA: Prentice-Hall, 1991.

[19] M. Trumić, K. Jovanović, and A. Fagiolini, "Decoupled nonlinear adaptive control of position and stiffness for pneumatic soft robots," *Int. J. Robot. Res.*, vol. 40, no. 1, pp. 277–295, Jan. 2021.

[20] Y. Huo, X. Li, X. Zhang, X. Li, and D. Sun, "Adaptive intention-driven variable impedance control for wearable robots with compliant actuators," *IEEE Trans. Control Syst. Technol.*, vol. 31, no. 3, pp. 1308–1323, May 2023.

[21] M. Trumic, C. della Santina, K. Jovanovic, and A. Fagiolini, "Adaptive control of soft robots based on an enhanced 3D augmented rigid robot matching," in *Proc. Amer. Control Conf. (ACC)*, May 2021, pp. 4991–4996.

[22] B. Siciliano et al., "Robotics and the handbook," in *Handbook of Robotics*. Cham, Switzerland: Springer, 2016, pp. 1–6.

[23] L. Sciavicco, *Modelling and Control of Robot Manipulators*. Cham, Switzerland: Springer, 2001.

[24] F. Flacco and A. De Luca, "Stiffness estimation and nonlinear control of robots with variable stiffness actuation," *IFAC Proc. Volumes*, vol. 44, no. 1, pp. 6872–6879, Jan. 2011.

[25] Natural Machine Motion Initiative. *Qbmove Maker Pro*. Accessed: Feb. 15, 2022. [Online]. Available: http://www.naturalmachinemotioninitiative.com/qbmovev01

[26] T. Ménard, G. Grioli, and A. Bicchi, "A stiffness estimator for agonistic–antagonistic variable-stiffness-actuator devices," *IEEE Trans. Robot.*, vol. 30, no. 5, pp. 1269–1278, Oct. 2014.

[27] S. Sen, S. Chatterjee, and C. Har, "Design and impedance estimation of a biologically inspired flexible mechanical transmission with exponential elastic characteristic," in *Proc. IEEE/RSJ Int. Conf. Intell. Robots Syst.*, Nov. 2013, pp. 5425–5430.

[28] A. Jafari, N. G. Tsagarakis, I. Sardellitti, and D. G. Caldwell, "How design can affect the energy required to regulate the stiffness in variable stiffness actuators," in *Proc. IEEE Int. Conf. Robot. Autom.*, May 2012, pp. 2792–2797.

[29] A. Jafari, "Coupling between the output force and stiffness in different variable stiffness actuators," *Actuators*, vol. 3, no. 3, pp. 270–284, Aug. 2014.

[30] A. Jafari, H. Q. Vu, and F. Iida, "Determinants for stiffness adjustment mechanisms," *J. Intell. Robotic Syst.*, vol. 82, nos. 3–4, pp. 435–454, Jun. 2016.

[31] J. R. Silvester, "Determinants of block matrices," *Math. Gazette*, vol. 84, no. 501, pp. 460–467, Nov. 2000.

[32] D. S. Bernstein, *Matrix Mathematics: Theory, Facts, and Formulas*. Princeton, NJ, USA: Princeton Univ. Press, 2009.

[33] R. Kelly, "Global positioning of robot manipulators via PD control plus a class of nonlinear integral actions," *IEEE Trans. Autom. Control*, vol. 43, no. 7, pp. 934–938, Jul. 1998.

[34] H. Khalil, *Nonlinear Systems* (Pearson Education). Upper Saddle River, NJ, USA: Prentice-Hall, 2002.

[35] J. Zhao, Y. Lv, Q. Zeng, and L. Wan, "Online policy learning-based output-feedback optimal control of continuous-time systems," *IEEE Trans. Circuits Syst. II, Exp. Briefs*, vol. 71, no. 2, pp. 652–656, Feb. 2024.

[36] W. Qi, S. E. Ovur, Z. Li, A. Marzullo, and R. Song, "Multi-sensor guided hand gesture recognition for a teleoperated robot using a recurrent neural network," *IEEE Robot. Autom. Lett.*, vol. 6, no. 3, pp. 6039–6045, Jul. 2021.

[37] Y. Huo, P. Li, D. Chen, Y.-H. Liu, and X. Li, "Model-free adaptive impedance control for autonomous robotic sanding," *IEEE Trans. Autom. Sci. Eng.*, vol. 19, no. 4, pp. 3601–3611, Oct. 2022.

[38] B. Siciliano et al., *Robotics: Modelling, Planning and Control*. Cham, Switzerland: Springer, 2010.

[39] A. Chaillet and A. Loría, "Uniform semiglobal practical asymptotic stability for non-autonomous cascaded systems and applications," *Automatica*, vol. 44, no. 2, pp. 337–347, Feb. 2008.

[40] M. Trumic, G. Grioli, K. Jovanovic, and A. Fagiolini, "Force/torque-sensorless joint stiffness estimation in articulated soft robots," *IEEE Robot. Autom. Lett.*, vol. 7, no. 3, pp. 7036–7043, Jul. 2022.

[41] R. Mengacci, F. Angelini, M. G. Catalano, G. Grioli, A. Bicchi, and M. Garabini, "Stiffness bounds for resilient and stable physical interaction of articulated soft robots," *IEEE Robot. Autom. Lett.*, vol. 4, no. 4, pp. 4131–4138, Oct. 2019.

Open Access funding provided by 'Università degli Studi di Palermo' within the CRUI CARE Agreement